ORIGINAL PAPER

# Kinesin velocity increases with the number of motors pulling against viscoelastic drag

Jason Gagliano · Matthew Walb · Brian Blaker ·
Jed C. Macosko · George Holzwarth

**Abstract** Although the properties of single kinesin molecular motors are well understood, it is not clear whether multiple motors pulling a single vesicle in a cell cooperate or interfere with one another. To learn how small numbers of motors interact, microtubule gliding assays were carried out with full-length *Drosophila* kinesin in a novel motility medium containing xanthan, a stiff, water-soluble polysaccharide. At 2 mg/ml xanthan, the zero-shear viscosity of this medium is 1,000 times the viscosity of water, similar to cellular viscosity. To mimic the rheological drag force on the motors when attached to a vesicle in a cell, we attached a 2 μm bead to one end of the microtubule (MT). During gliding assays in our novel medium, the moving bead exerted a drag force of 4–15 pN on the kinesins pulling the MT. The velocity of MTs with an attached bead increased with MT length and with kinesin concentration. The increase with MT length arose because the number of motors is directly proportional to MT length. Our results show that small numbers of kinesins cooperate constructively when pulling against a viscoelastic drag. In the absence of a bead but still in the viscous medium, MT velocity was independent of MT length and kinesin concentration because the thin MT, like a snake moving through grass, was able to move between xanthan molecules with little resistance. A minimal shared-load model in which the number of motors is proportional to MT length fits the observed dependence of gliding velocity on MT length and kinesin concentration.

## Introduction

Kinesin-1 is a member of a family of motor proteins that convert the chemical energy of ATP hydrolysis into the mechanical work of vesicle transport in cells. Kinesin-1 or conventional kinesin is a heterotetrameric protein consisting of two heavy chains (KHC) and two light chains (KLC). Kinesin-1 plays a central role in the transport of vesicles toward the (+)ends of microtubules, for example along axons.

In vitro experiments at 25°C have established that a single kinesin-1 motor can move cargo at a maximum average velocity of 800 nm/s, and kinesin-1 has an average velocity of 780 nm/s in COS cells (Cai et al. 2007). However, the maximum speed of small vesicles in cells is 3,500–4,000 nm/s (Allen et al. 1982; Schliwa 2003; Zhou et al. 2001). With better spatial and time resolution, the 800 nm/s average velocity is revealed to be the result of a series of quick 8 nm steps, each step taking only 15–50 μs, while the time between steps is 10 ms (Carter and Cross 2005; Nan et al. 2008; Svoboda et al. 1993). The ATP hydrolysis cycles of the two heads, and their synchronization to coordinate the binding and release of the heads to the MT, are understood in some detail (Klumpp et al. 2004), as is the dependence of velocity on opposing force. The motor stalls at $F_{ext} = 5$–7 pN (Coppin et al. 1997; Kojima et al. 1997; Visscher et al. 1999).

In contrast to single motors, multiple kinesins pulling a single vesicle or load are poorly understood. Measurements of velocity and stall force in several different types of cells suggest that motors of the same kind usually cooperate

J. Gagliano · M. Walb · B. Blaker · J. C. Macosko ·
G. Holzwarth (✉)
Department of Physics, Wake Forest University, PO Box 7507,
Winston-Salem, NC 27109, USA
e-mail: gholz@wfu.edu

constructively (Ashkin et al. 1990; Hill et al. 2004; Kural et al. 2005; Levi et al. 2006; Shtridelman et al. 2008, 2009; Welte et al. 1998). However, the velocity of kinesin-driven lipid droplets in *Drosophila* embryos decreases slightly when the number of motors increases from 1 to 2, suggesting that the motors interfere in this case (Shubeita et al. 2008).

In vitro motility assays with multiple kinesin motors have also failed to converge to a unique description. In the absence of opposing force, the average velocity in vitro is independent of the number density of motors over a wide range (Howard et al. 1989). However, at very high motor densities, velocity decreases (Beeg et al. 2008; Bieling et al. 2008).

To better define the number of motors, Diehl and coworkers linked two kinesin-1 motors to a scaffold, then linked the two-motor assembly to a quantum dot. In the absence of load, the velocities of one-motor and two-motor assemblies were identical, but analysis of run-length distributions showed that the two motors interfered with one another (Rogers et al. 2009). Crevenna et al. have shown that the 60 aa hinge-1 domain of kinesin-1 is necessary for cooperation between motors; motors lacking this domain move more slowly at even modest kinesin surface density (Crevenna et al. 2008). Multiple kinesin motors lacking the terminal 400–500 aas of its stalk and tail interfere strongly at high concentration (Bieling et al. 2008).

Hunt and coworkers have determined a force-velocity curve for 1 kinesin working against a viscous load (Hunt et al. 1994) and found it to be similar to single-motor force-velocity curves measured with an optical trap. When the kinesin density was increased by a factor of 1,800, the velocity increased to the "no-load" speed. This shows that a large number of kinesins can cooperate against a viscous load, but leaves uncertain how a small number perform.

To elucidate how a small number of motors function together with and without load in a viscous medium, we have now carried out kinesin-1 gliding assays against a 4–15 pN drag force at low kinesin densities. We use a dilute solution of xanthan to increase the viscosity to 1 Pa·s, 1,000 times the viscosity of water. By attaching a 2 μm bead to the MT, as shown in Fig. 1, gliding assays can be carried out against a drag force of 4–15 pN. This is comparable to the drag on vesicles undergoing fast transport in cytoplasm of cells (Ashkin et al. 1990; Hill et al. 2004; Shubeita et al. 2008; Welte et al. 1998). We find that the gliding velocity increases with MT length. This shows that small numbers of motors can move a cargo faster than a single motor can, if there is significant opposing drag. In the absence of a bead, but still at low kinesin concentration, the velocity is independent of kinesin concentration and MT length, in harmony with earlier studies at much higher kinesin concentration (Hunt et al. 1994). We show that a
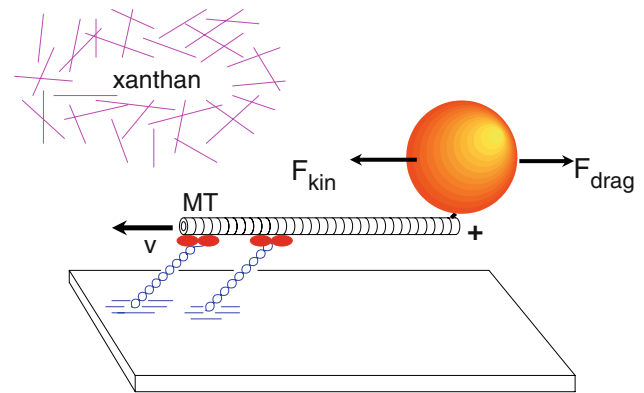


**Fig. 1** Diagram of the gliding assay for kinesin motility against the load of viscous drag. Two kinesin molecules (*blue* stalks, *red* motors) are shown with their tails adsorbed to a slide. In the presence of ATP, the motors step toward the (+)end of the MT, pulling it left. A bead (*orange*) is attached by a biotin-streptavidin linkage to the (+)end of the MT. It is subject to two forces: $F_{kin}$ is provided by the motors, $F_{drag}$ by the viscous fluid on the bead. The fluid, a mixture of buffer and stiff xanthan molecules (*magenta*), is shown in the *upper-left corner*

minimal shared-load model, in which the number of motors is proportional to the MT length, quantitatively explains the observed increase in MT gliding velocity with MT length.

## Materials and methods

### Kinesin

Kinesin-1 heavy chain (KHC) was prepared from plasmid pPK113 as described by Coy et al. (1999). The six histidine-tagged *Drosophila* kinesin-1 heavy chain (987 aa, 111,862 Da per monomer) was separated from other soluble proteins by Ni-NTA chromatography (Qiagen). The average yield was about 0.2 mg per g of wet cells. SDS-PAGE of the purified protein showed a single band at $115 \pm 5$ kDa.

### Fluorescently labeled MTs with (+)end biotin labeling

Fluorescent microtubules were prepared by copolymerizing rhodamine-labeled bovine tubulin ($T_R$) with unlabeled bovine tubulin ($T_0$), both from Cytoskeleton (Denver, CO). To begin polymerization, a 4 mg/ml tubulin mixture containing 4% $T_R$ and 96% $T_0$, dissolved in BRB80 + 1 mM DTT + 1 mM GTP, was warmed to 37°C for 5 min; BRB80 is 80 mM PIPES, 1 mM EGTA, 1 mM MgCl$_2$, pH 6.9. A 1/10 volume of 4 μM taxol (paxlitaxel, Sigma) was added while keeping the sample at 37°C. After 10 min, an additional 1/10 volume of 40 μM taxol was added. Finally, after an additional

10 min, a 1/10 volume of 400 µM taxol was added. The addition of taxol in logarithmically increasing concentrations is described by Mitchison (http://mitchison.med.harvard.edu/protocols.html). The microtubules were then sheared with a 10 µl glass syringe and diluted by a factor of 10 with BRB80 + 1 mM GTP + 1 mM DTT + 60 µM taxol. The resultant MTs were 2–20 µm long and fluorescently speckled (Chisena et al. 2007; Waterman-Storer and Salmon 1998).

Biotin-labeled bovine tubulin (0.7 mg/ml, Cytoskeleton, Denver, CO) was added to an approximately equal volume of the sheared MT solution and allowed to react for 15 min at 37°C. This added short biotin-labeled tails to the long speckled MTs. Most tails were at the (+)end of the MT because the rate of addition of tubulin dimers to the (+)end of a MT is twice that at the (−)end (Walker et al. 1988). Conveniently, the biotin-labeled tails were lightly labeled with rhodamine from the small residue of unpolymerized rhodamine-labeled tubulin that mixed with the non-fluorescent, biotin-labeled tubulin, making it easy to verify (+)end labeling (see Fig. 3).

Motility assays

Gliding assays for kinesin velocity were performed in microfluidic flow chambers composed of an acid-washed microscope slide, an 18 × 18 mm acid-washed coverslip, and two spacers cut from double-sided Scotch tape. The inside dimensions of the chamber were 18 × 5 × 0.06 mm. The chamber was filled by capillary action; 10–20 µl liquid was added to one open end while fluid was wicked from the other end with a small piece of filter paper. First, 20 µl of a solution containing 0.5 mg/ml casein (Fisher) in BRB80 was introduced into the chamber to coat the coverslip, followed by 10 µl of 20 µg/ml kinesin. After 5 min, 20 µl of a solution containing microtubules in motility solution (BRB80, 1 mM Mg-ATP, 6 mM MgCl$_2$, 18 µM taxol, plus an oxygen scavenging system) was added. The oxygen-scavenging system was 40 mM D-glucose, 0.02 mg/ml catalase, 0.04 mg/ml glucose oxidase, and 60 mM BME. After 2 min, we flowed in 20 µl of a solution containing 2-µm-diameter streptavidin-coated polystyrene beads (Polysciences, Warrington, PA) suspended in motility buffer supplemented with different concentrations of purified xanthan. The open ends of the chamber were then sealed with food-grade grease (Mobil FM102, Exxon-Mobil, Houston, TX). Images were recorded at 8.3 frames/s and stored in digital form for later tracking.

Kinesin concentration was determined by Bradford assays. The surface density of motors was 1,000 motors/µm$^2$ for "high" surface density and 250 motors/µm$^2$ for "low" density. These Bradford numbers assumed that all injected kinesin adhered to the surface of the sample chamber and 100% of the adhered protein was active, so the Bradford number probably overestimates the true number density of active motors. Probably a better measure of the surface density of kinesin in our experiments is that at "low" motor concentration in the absence of xanthan, short MTs (2–5 µm) frequently swiveled about a point along their axis. Swiveling is a clear indication that the MT is bound to the coverslip by a single motor (Leduc et al. 2007). At "high" motor concentration, swiveling was rarely observed, even for the shortest microtubules.

Xanthan

Xanthan is a widely used water-soluble bacterial exopolysaccharide with a broad molecular weight distribution. $M_w$ is between $1 \times 10^6$ and $7 \times 10^6$. In its native form, which is probably double-stranded, xanthan is about as stiff as DNA. At a concentration of 2 mg/ml, xanthan has a viscosity of about 1 Pa·s at low shear rate (Milas et al. 1985; Rodd et al. 2000). Beads of diameter 160 nm experience a similar effective viscosity, 0.5–1 Pa·s when suspended within the cytoplasm of live fibroblasts (Luby-Phelps 2000).

*Purification*

Purification proceeded according to the methods of Holzwarth (1976) and Jeanes et al. (1961). Xanthan powder (Keltrol, CP-Kelco, San Diego, CA) was dissolved at a concentration of 1 mg/ml by overnight stirring in deionized water at 5°C. KCl (0.34 M) and EDTA (0.0025 M) were added, and the pH was adjusted to 7.0. Ethanol was added dropwise to reach a volume fraction of 0.2. The viscous but hazy solution was centrifuged for 4 h at 34,000g to remove undissolved polymer and cellular debris. Additional ethanol was added dropwise to the clear solution until precipitation occurred at approximately 0.32 v/v. The precipitated polymer was redissolved in 80 mM PIPES, pH 6.9, to a nominal concentration of 2.5 mg/ml, centrifuged to remove undissolved polymer, prefiltered, filtered through a 0.45 µm syringe filter, then dialyzed against 80 mM PIPES, 1 mM EGTA, pH 7.0. This purified stock solution was clear.

The concentration of xanthan in the purified stock solution was determined by the phenol-H$_2$SO$_4$ carbohydrate test (Dubois et al. 1956), with glucose as a parallel standard. Results were corrected for the fact that the absorbance of glucose is 1.43 times larger than the absorbance of an equal weight concentration of xanthan (Holzwarth 1976). The purified xanthan stock was stored at 5°C.

To determine the viscosity of xanthan solutions from the Brownian motion of beads, the density of the xanthan

samples was increased to 1.06 g/ml by adding 8% KCl. Two-micrometer polystyrene beads (Polysciences, Warrington, PA, density 1.06 g/ml) were then added, and the suspension was flowed into a simple "micro fluidic" sandwich cell made from a microscope slide "bottom," two narrow strips of double-sided Scotch tape as sides, and a coverslip as "top." After sealing the ends with grease, 1,000-image data sets were recorded at 8.3 frames/s with a Nikon E600 microscope with 60× oil immersion objective (NA 1.4), DIC optics, and a Hamamatsu Orca ER camera. We were careful to focus it midway between the top and bottom surfaces of the sample chamber to avoid wall effects. Beads did not settle because the bead density matched the solution density.

### Effective viscosity of xanthan solutions

The mean-squared displacement (MSD) of the beads suspended in xanthan solutions was calculated for time intervals of 0.12–100 s. The effective viscosity $\eta$ as well as the viscoelastic moduli $G'$ and $G''$ were determined from the MSD by Mason's Generalized Stokes-Einstein analysis procedure (Mason 2000). Figure 2 shows the effective viscosity for xanthan concentrations of 0.5–2.0 mg/ml.

As a control, the viscosity of water was determined in the same way. The results, shown in Fig. 2, agree with the Handbook value of the viscosity of water at 25°C, $0.88 \times 10^{-3}$ Pa·s.

### Particle tracking

The positions of beads at the ends of MTs were determined to approximately ±0.05 pixel precision by one of two



**Fig. 2** The viscosity of xanthan solutions, as determined from the Brownian motion of 2-μm beads. The xanthan concentrations (*top to bottom*) are 2, 1.5, 1, 0.5, and 0 mg/ml. Solvent is 80 mM PIPES, 8% KCl, pH 6.9, $T = 25$°C. The abscissa is the shear rate $1/\tau$

programs. Video Spot Tracker, a Matlab program written by Russell Taylor and his colleagues at the University of North Carolina-Chapel Hill worked best with beads. The program is available at http://www.cs.unc.edu. We added Matlab code to correct for stage drift by subtracting the motion of the center-of-mass of the 5–8 beads, which could be tracked within each movie.

MTs were tracked by a subpixel pattern-matching algorithm in the Odyssey Native Language or MIL 8.0 running on a Matrox Odyssey image-processing board (Matrox, Dorval PQ, Canada). MTs were speckled to improve the precision of the velocity determination (Chisena et al. 2007).

## Experimental results

### MTs with beads attached to their (+)ends

Upside-down motility assays were carried out against a viscoelastic load by adding small amounts of the stiff, high-molecular-weight, negatively charged bacterial exo-polysaccharide xanthan to the motility buffer. Adding a few milligrams per milliliter of xanthan increases the viscosity of water by a factor of 1,000–10,000 when measured by a conventional rheometer (Milas et al. 1985). However, a gliding MT would not experience this high viscosity because it can reptate between the polysaccharide chains. To increase the drag force on the kinesin motors propelling MTs in a gliding assay, a 2- or 6-μm streptavidin-coated bead was attached to the (+)ends of the MTs. To achieve attachment to the (+)end only, we added biotin-labeled, nonfluorescent tubulin to previously polymerized, fluorescently labeled MTs. The biotin-labeled tubulin added preferentially to the (+)end of the preexisting MTs (Walker et al. 1988). The resultant MTs had strong fluorescence intensity over most of their length and weak fluorescence in the biotin-labeled tail section. The weak fluorescence in the tail arose from small amounts of fluorescent tubulin remaining in the reaction mixture when the biotin-labeled tubulin was added.

In Fig. 3, we show two "movies" of our biotin-capped MTs gliding on a carpet of full-length *Drosophila* kinesin adsorbed to casein-coated glass. The left half shows several MTs with a weakly fluorescent tail at the end of a heavily fluorescent filament. Its time sequences show that the weakly fluorescent section was almost always at the trailing (+)end of the gliding MT. The right side shows a corresponding "movie" of similar MTs after streptavidin-coated beads were added. Almost without exception, the beads were bound to the trailing (+)ends of gliding MTs (Fig. 3). By keeping the MT and bead concentrations low, each MT carried either no bead or one bead.
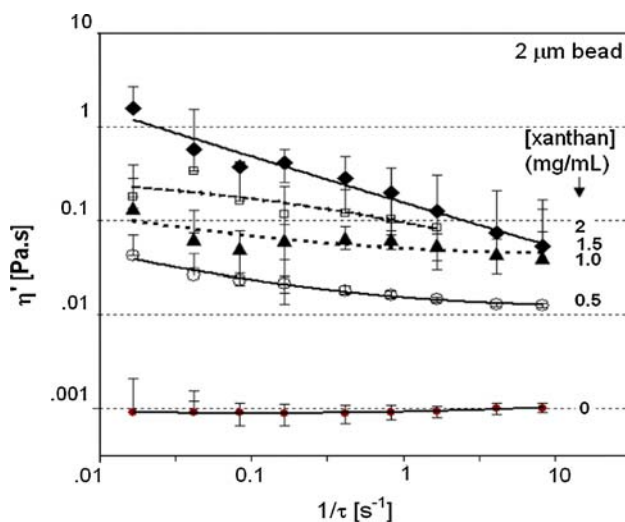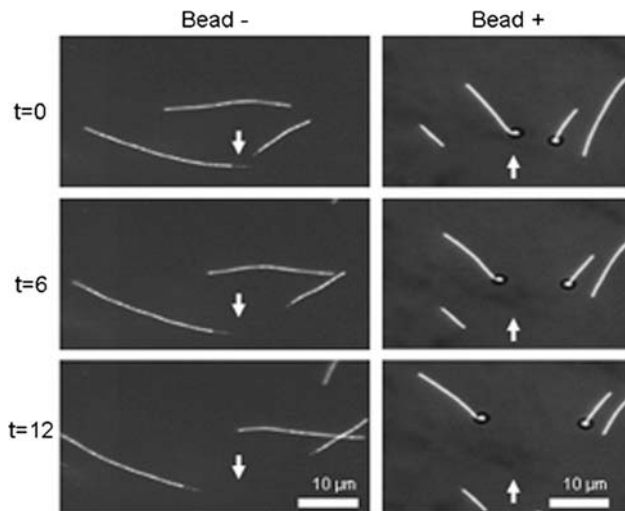
**Fig. 3** Time sequences of fluorescent MTs with biotin labels at their (+)ends. Most of the length of each MT is strongly fluorescent but biotin-free. The short biotin-labeled tail has reduced fluorescence intensity but is still visible. *Left side* MTs without a bead. The *arrow* at $t = 0$ points to a tail. The *arrow* remains in its original location in the subsequent images as a reference point. *Right side* MTs with a bead. The time-sequences show that the biotin end is at the trailing (+)end of the MTs. The *arrow* at $t = 0$ points to a bead at the end of an MT. Conditions: 1 mM ATP, 25°C, 60×/NA 1.4 oil objective, 12-bit cooled Hamamatsu ORCA ER camera with $6 \times 6$ μm pixels

Effect of xanthan concentration on gliding velocity

We next had to establish the optimum xanthan concentration to generate physiologically appropriate drag on the bead. For a 2-μm bead moving at 500 nm/s through a medium with $\eta = 1$ Pa·s, Stokes's Law gives the drag force as:

$$F_{\text{drag}} = 6\pi\eta r v = 9.4\,\text{pN} \tag{1}$$

This force is reasonable; it is above the 8 pN stall force for one kinesin motor but less than the expected stall force for two motors. The assumed viscosity, 1 Pa·s, corresponds approximately to the low-shear viscosity of PC12 and NT2 cells, two live-cell systems whose viscoelasticity we have studied (Hill et al. 2004; Shtridelman et al. 2008). It also corresponds to the low-shear viscosity of 2 mg/ml xanthan solutions (Fig. 2).

We measured the gliding velocity of MTs through xanthan solutions with concentrations of 0–3 mg/ml, with and without a bead, for 2- and 6-μm beads (Fig. 4). MTs without a bead moved at 720 nm/s, the control velocity for full-length *Drosophila* kinesin, regardless of xanthan concentration. This is understandable: gliding MTs can reptate between the xanthan chains.

MTs pulling a 2-μm bead moved significantly more slowly as the xanthan concentration increased from 0 to 3 mg/ml (Fig. 4, middle curve). In the absence of xanthan,
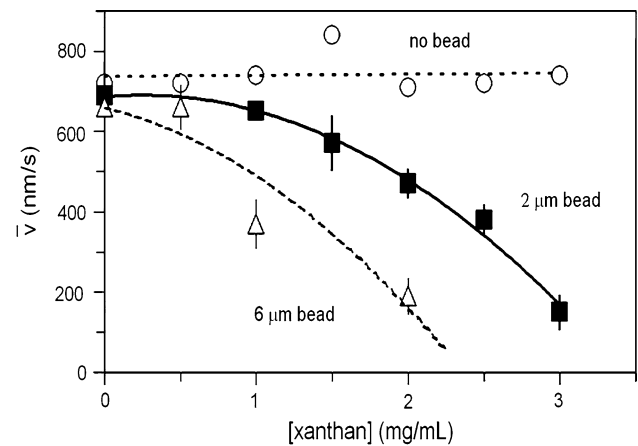


**Fig. 4** Average velocity of MTs as a function of xanthan concentration during upside-down gliding assays powered by *Drosophila* KHC. The three curves correspond to MTs carrying no bead, a single 2-μm bead, or a single 6-μm bead. MTs with a 6-μm bead did not move if [xanthan] = 3 mg/ml. [ATP] = 1 mM. $T = 25$°C. The kinesin surface density was 100–1,000 motors/μm², based on Bradford assay. The surface density of active motors is almost certainly less

the MTs with a bead moved at the same velocity, 720 nm/s, as MTs without a bead. This suggests that the mass of the bead did not interfere with kinesin.

MTs pulling a 6-μm bead moved even more slowly in the presence of xanthan (Fig. 4, lower trace). Stokes's Law predicts that the drag force on a 6-μm bead is three times greater than the drag on a 2-μm bead. The observed decrease in velocity was approximately a factor of two. From the results in Fig. 4, we concluded that 2 mg/ml xanthan and 2-μm beads would provide a reasonable "sweet spot" for further studies on the effect of MT length on gliding velocity.

Effect of MT length on gliding velocity at fixed xanthan concentration

The lengths of individual MTs were easily determined from the video microscope images taken with a 60× objective (Fig. 3). The average MT length in a given sample was controlled by varying the number of times the sample was forced through a fine syringe needle. We saved movies of 200 frames (24 s) and determined the length $L$ and average velocity of specific MTs in each movie by post processing. Within a particular assay, about 80% of the MTs lacked a bead, while 20% in the same field had a single 2-μm bead at one end.

In the absence of a bead, all MTs moved at the control speed, regardless of their length or the kinesin concentration (Fig. 5, black triangles and black diamonds). However, short MTs pulling a bead moved much more slowly, while
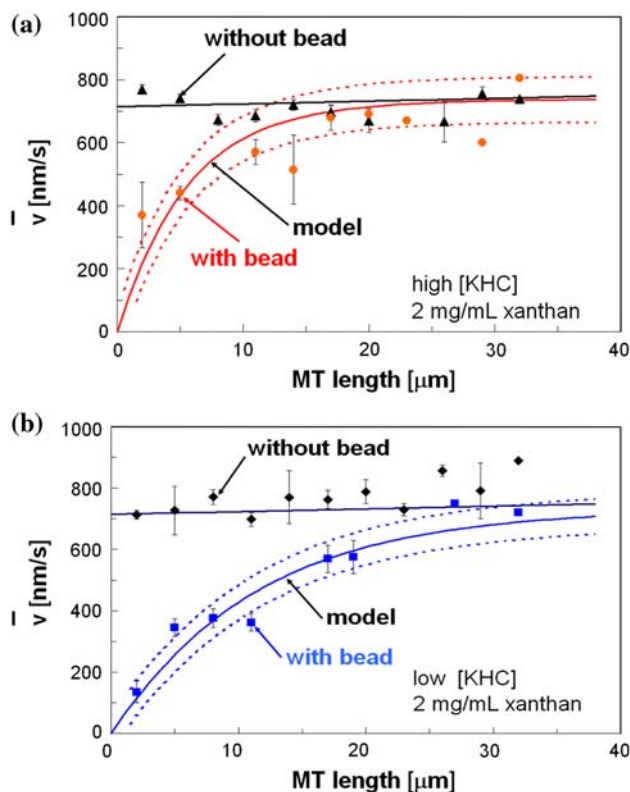
Fig. 5 Average gliding velocity of MTs in motility buffer containing 2 mg/ml xanthan, with and without a 2-μm bead. *Panel* **a** high kinesin concentration. *Black triangles* MTs without bead. The *black line* is a least-squares fit of a straight line through the "no bead" data at both high and low kinesin concentrations. *Red circles* MT pulling a 2-μm bead. The *solid red line* is a least-squares fit of the shared load model to the experimental data. The *fine dotted lines* on either side of the model line mark ±1 standard deviation. *Panel* **b** low kinesin concentration (1/4th of high concentration). *Black diamonds* MTs without bead. *Blue squares* MTs with bead. The *solid blue line* is a least-squares fit of the shared load model to the data. The *fine dotted lines* mark ±1 standard deviation from the model line. *Error bars* are ±SEM

MTs with $L \geq 20\,\mu\text{m}$ moved at the control speed (Fig. 5, red circles and blue squares). In addition, the velocity of short MTs with a bead was lower for low kinesin concentration. These observations support the idea that the increased velocity of longer MTs arose from an increase in the number of attached motors.

To further evaluate this idea quantitatively, we tested whether the observed trends of velocity with MT length (Fig. 5) were consistent with the predictions of a minimal shared-load model, which is described in the next section. This model was previously used to derive an expression for velocity $v$ as a function of opposing force $F$ for a fixed number of motors $n$ (Hill et al. 2004) and can easily be rewritten to provide $v$ as a function of $n$ for fixed $F$. To test whether the model fits the current data, in which velocity varies with length $L$, we need a relation between $n$ and $L$.

The obvious relation is $n = wL$, where $w$ is the number of motors per micron of MT length. This relation is reasonable at small values of $n$, when only a small fraction of the binding sites on the MT are occupied.

Assuming that $n = wL$, the shared-load model gives $v_F(L)$ in analytic form, with $w$ as the only adjustable parameter. This parameter was evaluated by a least-squares fit of $v_F(L)$ to the experimental data (solid curves labeled "model" in Fig. 5). For high kinesin concentration, $w = 0.35 \pm 0.03$ motors/μm, and six out of eight data points are within $\pm\sigma$ of the model trendline. For low kinesin concentration, $w = 0.17 \pm 0.02$ motors/μm, and five out of eight data points are within $\pm\sigma$ of the model trendline. The factor-of-two ratio between the fitted values of $w$ compares favorably to the expected factor-of-four from the concentration ratio. Although there is scatter in the data, the overall fit to the model supports the idea that the velocity of a gliding MT increases with an increase in the number of motors if the opposing force is close to a physiologically relevant load.

The values of $w$ obtained in the fits provide a scale relating $n$ to $L$. This tells us that $n = 1$ when $L = 2.9\,\mu\text{m}$ at our "high" kinesin concentration, and $n = 1$ for $L = 6\,\mu\text{m}$ for our "low" concentration, which is ¼ of "high". Consistent with these values is the observation that in gliding assays at low kinesin concentration but without xanthan, MTs with $L \leq 5\,\mu\text{m}$ swiveled about a point somewhere along their axes. Such swiveling is a clear signal that $n = 1$ (Leduc et al. 2007).

## "Instantaneous" MT velocity

The velocity data shown in Figs. 4 and 5 are average velocities over 18–24 s. A striking feature of the individual tracks is that the velocity often changed abruptly over intervals of 1–4 s. We have observed a similar pattern in vivo (Hill et al. 2004; Macosko et al. 2008; Shtridelman et al. 2008, 2009) and suggested that the changes in slope could arise from changes in the number of motors. Figure 6 shows tracks for several MTs, with and without a bead, in the presence of 2 mg/ml xanthan.

To test whether the apparent changes in slope were statistically supported, we carried out a least-squares fit of a series of straight lines, connected at their ends, to the data. The adjustable parameters in the fit were the number of segments $N_{\text{seg}}$, the times at which the slope changed, and the slope of each segment. The Matlab function "fmincon" was the computational engine behind the fitting process. Our Matlab program was fully automatic except for the choice of $N_{\text{seg}}$. The optimum value of $N_{\text{seg}}$ was selected by the minimum, or a sharp drop, in a plot of the goodness-of-fit parameter $\chi^2_{\text{red}}$ against $N_{\text{seg}}$ (Bevington 1969). The "best fits" are plotted with the experimental data in Fig. 6. The
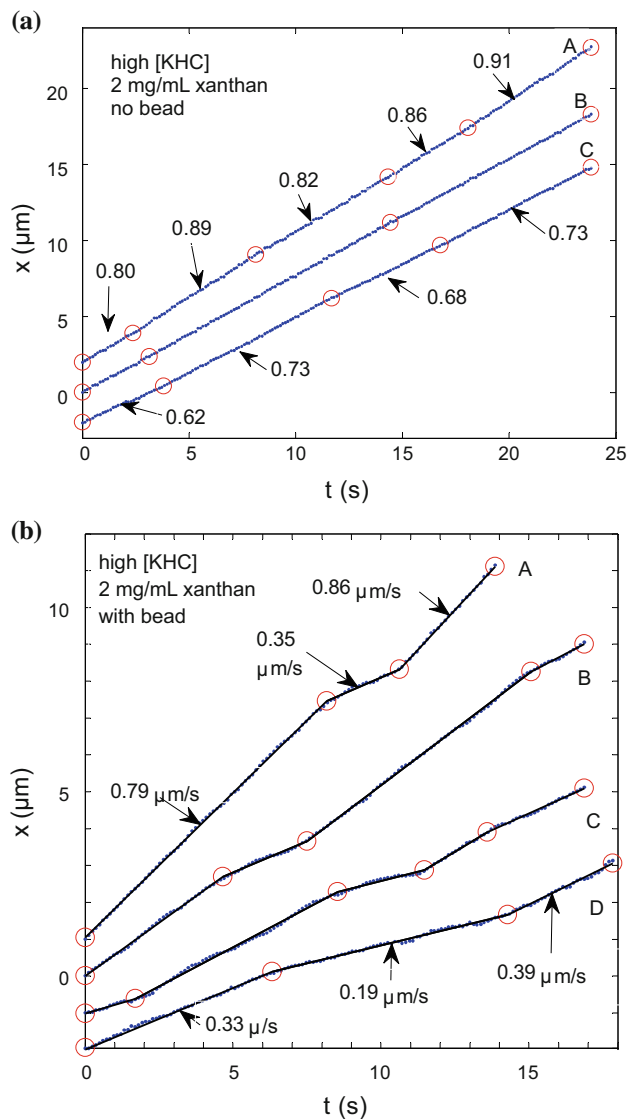
**(a)**



**(b)**



**Fig. 6** Position along the path of a MT as a function of time during motility assays in 2 mg/ml xanthan. Position data are given by *blue dots*, with one dot per frame (0.120 s). Data were fitted to a set of connected straight lines, shown by *black lines*. The *red circles* mark times at which the fitting program detects a velocity change. Velocities (slopes) of fitted straight-line segments are given in μm/s. *Panel **a*** no bead. The values of $\chi^2_{red}$ for the fits are 0.68, 0.45, and 0.44 for *A*, *B*, and *C*, indicating strong statistical significance for the straight-line model. The *black fitted lines* are deleted for clarity because they obscure the data. *Panel **b*** with bead. The values of $\chi^2_{red}$ for the fits are 0.39, 0.54, 0.72, and 0.44 for *A* through *D*. The *blue data points* are hard to detect in the presence of the *fitted black lines* because they overlap to a great extent

values of $\chi^2_{red}$, which are given in the figure legend, were all substantially less than 1, showing that in every case, the linked-straight-lines model was statistically well supported (Bevington 1969). The velocity of the MT during each frame was taken from the slope of the fitted line at that time.

## Histograms of the instantaneous velocity

The number of motors moving a given microtubule will change with time when individual motors "fall off" the MT or reach its end. In the absence of significant load, average MT velocity does not change with the surface density of kinesin motors in gliding assays (Gibbons et al. 2001; Howard et al. 1989), and observable fluctuations in *v* for individual MTs would not be expected if *n* changes with time. However, in the presence of physiologically significant load, changes in *n* should lead to observable changes in *v*. The time scale for such changes can be estimated. First, a motor could "fall off" while moving along a long MT. The number of steps taken by a single kinesin-1 before falling off is about 100 at saturating [ATP] (Block et al. 1990; Hackney 1995). If the velocity under load is 400 nm/s, 100 steps take 2 s, suggesting that *v* should change at intervals of roughly 2 s. Second, a motor can reach the end of the MT. The average time for a single kinesin traveling at velocity *v* to reach the end of an MT of length *L* is *L/v*, assuming that the initial binding point is at the leading end. For *v* = 400 nm/s and *L* = 5 μm, the average time to reach the end is 12 s. These "back of the envelope" numbers suggest that if the average number of motors is small (e.g., 3), we may be able to observe fluctuations in the velocity when *n* increases to 4 or decreases to 2.

Histograms of the velocities for high and low kinesin concentration, with and without a bead, are shown in Fig. 7. At high kinesin concentration but no bead (upper panel), the velocity histogram was a narrow peak centered near 800 nm/s. However, when a bead was present, the velocity histogram was much broader, with velocities ranging between 0 and 800 nm/s. When the kinesin concentration was reduced (Fig. 7, lower panel), the velocity distribution without a bead broadened substantially.

At low kinesin concentration with a bead, the distribution shifted markedly to lower velocities. To test for the possibility of distinct peaks in the velocity histogram corresponding to 0, 1, 2…6 motors, the histograms were fitted with one to seven Gaussians. Each Gaussian was defined by three parameters: amplitude, location, and width. The amplitude and location were allowed to vary independently for each Gaussian. However, the widths of Gaussians 2…6 were forced to be identical to reduce the number of independent parameters. The optimum number of Gaussians was determined by the lowest value of $\chi^2_{red}$.

At low kinesin concentration, the lowest value of $\chi^2_{red}$ for the Gaussian fits occurred for five Gaussians, which are shown in Fig. 7, lower panel. The lowest $\chi^2_{red}$ was 10, a sign of weak statistical significance (Bevington 1969). Although the Gaussians are approximately equally spaced, their positions were allowed to vary independently in the
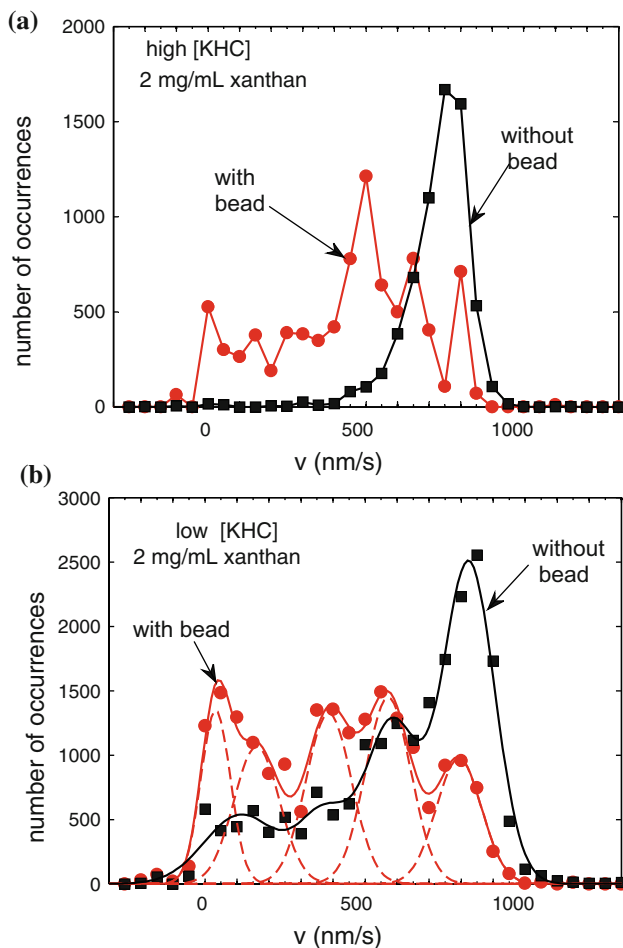
**(a)**



**(b)**



Fig. 7 Histograms of the instantaneous velocity of kinesin in 2 mg/ml xanthan, with and without an attached bead. *Upper panel* High kinesin concentration. Each frame is counted as an occurence. The number of MTs tracked was 45 with bead and 105 without bead. *Lower panel* Low kinesin concentration. The number of MTs tracked was 75 with bead and 105 without bead. 1 mM ATP, 25°C. The five Gaussians shown, which fit the data with $\chi^2_{red} = 10$, have amplitudes 1,409, 1,097, 1,334, 1,459, 977, centers 35, 162, 390, 573, 792 nm/s and widths 42, 69, 69, 69, 69 nm/s

fitting process. For high kinesin concentration (upper panel), no statistically significant fit to a set of Gaussians could be obtained.

### Effect of load and MT length on the duration of constant-velocity movement in the presence of xanthan

We tested whether MT length and the presence of a bead influenced the average duration $T_{seg}$ of the constant-velocity segments of tracks in 2 mg/ml xanthan, with and without a bead. MT length had almost no influence on $T_{seg}$ over the accessible MT length range of 2–35 μm (data not shown). MTs with an attached bead showed a longer average duration than MTs without a bead, at both low and
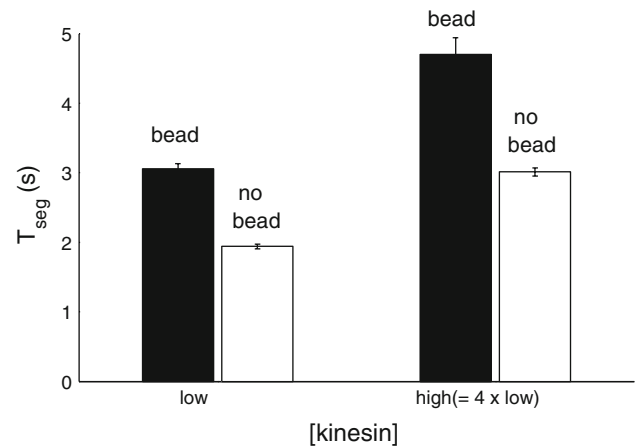


Fig. 8 Average duration T, in seconds, of the constant velocity segments during gliding assays in 2 mg/ml xanthan at low kinesin concentration (*left bars*) and high kinesin concentration (*right bars*) in the presence and absence of a 2-μm bead at the (+)end of the MT. The *error bars* are SEM. The numbers of MTs for the four bars, from *left* to *right*, are 105, 75, 45, and 105

high kinesin concentrations (Fig. 8). Note, however, that these results are sensitive to the selection of the "best" value for the number of segments, which was more difficult in the "no bead" case because the velocities of segments fell into a narrow range.

### Shared-load model

Velocity-force relations for multiple motors

Models can be helpful in understanding how several motors might interact to pull a single load. A minimal model is to assume that the load is shared equally between the attached motors. From the experimental force-velocity curve for one motor, the force-velocity curves for *n* motors can be calculated in analytic form (Hill et al. 2004). Adding a force-dependent unbinding rate and stochastic switches in motor number provides a specific mechanism for coupling between motors, which also predicts that velocity increases with number of motors in the presence of external load (Klumpp and Lipowsky 2005). It also predicts a strong increase in the walking distance with motor number. A model that allows nonequal load sharing predicts longer walking distance with motor number at high load (Kunwar et al. 2008).

We have used the minimal shared-load model to understand our results because the small number of parameters and analytic form of this model allowed us to apply standard least-squares fit methods to fit the experimental data (Fig. 5). The assumptions are:

1. *For 1 motor*, the dependence of average velocity $v_1$ on force $F_1$ is taken from experiment. We use the

constant-force optical trap velocity measurements of the Block group (Visscher et al. 1999). The experimental data were fitted to a quadratic equation:

$$v_1 = a_2 F_1^2 + a_1 F_1 + a_0 \qquad (2)$$

The fit was excellent ($R^2 > 0.99$) and provided values for $a_2$, $a_1$, and $a_0$.

2. *For n motors*, the total force $F_{total}$ is simply $nF_1$. That is, if $F_{total}$ is required to move a vesicle at velocity $v$, and $n$ dimeric motors are available, then each motor supplies force $F_{total}/n$. With these assumptions, the velocity $v_n$ for $n$ motors is

$$\vec{v}_n = a_2 \big(\vec{F}_{total}/n\big)^2 + a_1 \big(\vec{F}_{total}/n\big) + a_0 \qquad (3)$$

Figure 9 plots this equation for $n = 1$, 2, and 3. Note that the velocity is independent of the number of motors at low load, as observed experimentally (Howard et al. 1989).

### Velocity-force relation for viscous drag

The other force on the bead is viscous drag (Fig. 1). We rewrite Stokes's Law to relate the bead velocity to the drag force:

$$\vec{v} = -\vec{F}_{drag}/(6\pi\eta r) \qquad (4)$$

for a sphere of radius $r$ in a medium of viscosity $\eta$.

It is useful to plot the force-velocity curve of kinesin (Eq. 3) and the force-velocity curve of the drag force (Eq. 4) in the same graph (Fig. 9). The intersections between the Stokes's Law line and the motor curves, labeled X, Y, and Z in Fig. 9, mark the velocity at which the kinesin force equals the (magnitude of) the viscous force for one, two, and three motors.
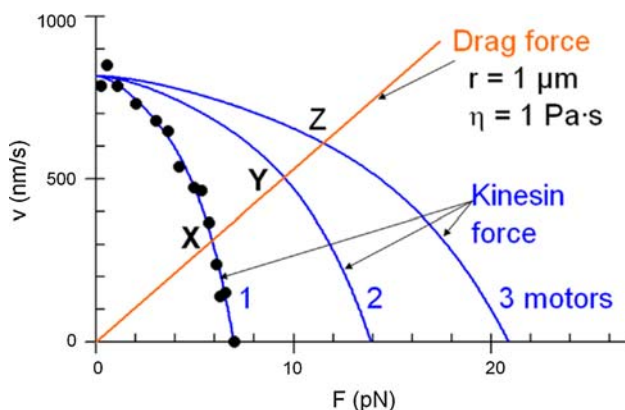
The choice of $\eta$ in Eq. 4 is complicated by the fact that both cytoplasm and xanthan solutions are shear-thinning. As an additional complication, kinesin moves in abrupt 8 nm steps (Kojima et al. 1997; Nan et al. 2008; Svoboda et al. 1993). These observations might suggest that the appropriate value of $\eta$ should correspond to a high shear rate. However, detailed analysis shows that the low shear-rate limit for $\eta$ is appropriate because the motion is processive and the medium is viscoelastic (Holzwarth et al. 2002).

### Dependence of velocity on the number of motors in the shared-load model

It is useful to reformulate the shared-load model to give $v$ as a function of $n$, the number of motors, for fixed $F$. Setting Eq. 3 equal to Eq. 4 and rearranging, we obtain the quadratic equation

$$\frac{a_2}{n^2}F^2 + \left(\frac{a_1}{n} - \frac{1}{6\pi\eta r}\right)F + a_0 = 0 \qquad (5)$$

This equation is easily solved for $F$ by standard methods. The physically meaningful root provides an analytic expression for $F(n)$. An analytic expression for $v(n)$ is obtained from $F(n)$ with the help of Eq. 4. The parameters $\eta$, $r$, $a_0$, $a_1$, and $a_2$ are fixed by experiment. The resultant dependence of velocity on $n$ is shown in Fig. 10 for a 2-μm diameter bead in a medium with $\eta = 1$ Pa·s (2 mg/ml xanthan).

The analytic form for $v(n)$, obtained by solving Eq. 5, was used in the "Experimental results" section to generate the trendlines through the observed measurements of velocity as a function of MT length $L$ for MTs pulling a



**Fig. 9** Velocity/force curves for the shared-load model. *Black circles* are measured velocities for kinesin at saturating ATP concentration (Visscher et al. 1999). The *blue line* for one motor is fitted through the data points. The *blue lines* for two and three motors are plots of Eq. 3 with $n = 2$ and $n = 3$. The *red line* is the Stokes's Law viscous drag (Eq. 4) on a 2-μm-diameter sphere in xanthan ($\eta = 1$ Pa·s)
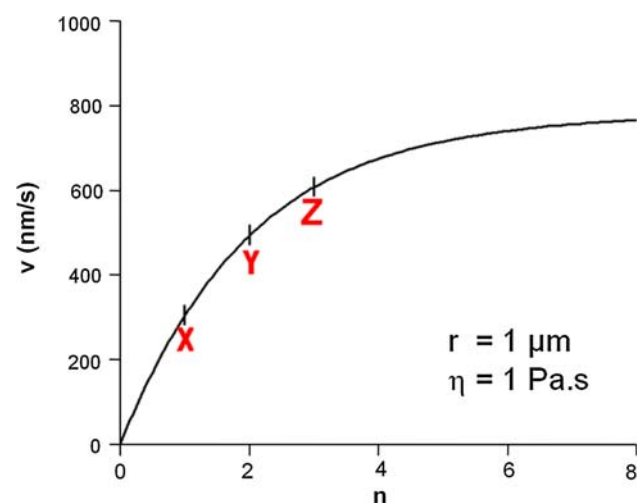


**Fig. 10** Velocities predicted by the shared-load model for 0–8 kinesin dimers. The load is provided by the drag of a 2-μm diameter sphere in a medium with $\eta = 1$ Pa·s. The points labeled X, Y, and Z, corresponding to $n = 1$, 2, and 3 kinesins, are also marked in Fig. 9

bead through xanthan solution (Fig. 5). The single adjustable parameter in those fits was $w$, the number of motors per unit length. A statistically significant difference in $w$ was observed with a fourfold difference in kinesin concentration.

## Discussion

The primary reason to determine the properties of kinesin in a viscous medium rather than with an optical trap is that viscous drag is probably the primary force against which work is done to move vesicles in cells. Unlike the force of an optical trap, viscous drag is proportional to velocity, so when the vesicle doesn't move, the opposing force vanishes. There is now abundant evidence that kinesin moves by executing approximately 100 abrupt steps per second. Each step takes only 15–35 μs in vitro (Carter and Cross 2005; Nishiyama et al. 2001) and 50–100 μs in vivo (Nan et al. 2008). Consequently, although the mean velocity may be 0.5–1 μm/s, the velocity must briefly spike to 60–150 μm/s during a step. Between steps, $v = 0$. The viscous drag is large during the brief kinesin steps and small (zero?) between steps. This consequence of the observed stepping behavior has been largely ignored but may be significant to signaling between the two heads of a single motor and to interactions between motors. Elasticity of the medium complicates the time-dependence of the opposing force (Holzwarth et al. 2002; Thomas and Walters 1965).

Gliding assays of single and multiple kinesins have been previously carried out in a viscous medium called visc-mix (Hunt et al. 1994). Visc-mix is 145 mg/ml trypsin inhibitor, 150 mg/ml dextran, and 75 mg/ml Ficoll. The viscosity is 100-fold the viscosity of buffer. Visc-mix exerts significant drag on the gliding MTs, unlike the 2 mg/ml xanthan solutions we have used. At kinesin surface densities of approximately 10 motors/μm², each moving MT is pulled by a single motor, regardless of length. The gliding velocity of MTs in visc-mix then decreases with increasing MT length because drag is proportional to MT length. The observed gliding velocities were used by Hunt et al. to determine a force-velocity curve for one kinesin working against the viscous drag of visc-mix. The measured curve is similar to the curve measured against the constant force of an optical trap.

When the surface density of kinesin is increased from 10 to 6,000 motors/μm², MT speed in visc-mix increases, becoming independent of MT length. Hunt et al. suggest that the increase in drag force with MT length is compensated by an increase in the number of motors. This is consistent with our results (Fig. 5).

The dependence of both motor number and viscous drag on MT length in the Hunt study complicates quantitative determination of the effect of motor number alone. The spherical bead that we attached to the end of the MT has a much larger drag than the MT in the medium we used. This clarified the effect of motor number on velocity. The bead was comparable in size to vesicles in cells. Unlike the snakelike MT, the bead could not reptate between the xanthan molecules. The bead thus experienced the drag predicted for a sphere by the solution's macroscopic viscosity (1 Pa·s). As a result, a small increase in the number of motors with MT length increased the velocity significantly, at constant kinesin surface density.

The use of Stokes's Law to calculate the force on the bead during gliding assays in xanthan has two potential problems, the "wall effect" and the "depletion layer effect." The wall effect arises because the gliding MT is only 17 nm away from the casein-coated surface during motility assays with kinesin-1 (Kerssemakers et al. 2006), whereas Stokes's Law is derived for a sphere in an unbounded medium. Since the MT diameter is 25 nm, a bead attached to the MT is at most $17 + 25 = 42$ nm above the stationary surface. The hydrodynamic effects of a nearby wall have been studied both experimentally and theoretically. The increase in force on a sphere is at most 33% (Kaiser et al. 2004).

In solutions of a stiff polymer such as xanthan, the polymer concentration is reduced near nonabsorbing walls because of steric exclusion. The mean depletion layer thickness $L$ has been measured for xanthan solutions of concentration 10–1,000 ppm (Ausserre et al. 1986). The value of $L$ is 25 nm at 1,000 ppm and decreases with increasing polymer concentration. Drag is less in the depletion layer. In our gliding assays, the MTs are within the depletion layer. However, most of the surface area of the 2-μm beads is exposed to the bulk xanthan concentration. This suggests that the depletion layer is unlikely to have a significant effect on the drag force in our experiments. In any case its effect is opposite that of the wall effect.

An inconsistency exists between the velocities for Gaussian peaks at $n = 1, 2, 3$ in the histograms (Fig. 7) and the velocities for $n = 1, 2, 3$ in the minimal shared-load model (Figs. 9, 10). The velocities of the peaks of the Gaussians in the histogram fall on a straight line when plotted against $n$, whereas the model predicts that the peaks should get closer together as $n$ increases. Further work is required to resolve these inconsistencies. The fact that the sudden changes in velocity every 1–3 s, previously observed in vivo, have now also been observed in vitro (Fig. 6) increases the likelihood that the same mechanism applies.

At least three factors differ between our in vitro system and vesicle transport in cells. The first is that the motors in our experiments are immobilized at random locations on the glass substrate, whereas kinesins attached to a

membrane can move within the membrane surface to bunch together (Leduc et al. 2004). It seems likely that cooperation between motors in cells would be affected by such bunching.

A second limitation is that our experiments were done with KHC tails adsorbed to a casein-coated glass surface, whereas in cells kinesin is attached to its load by a complex of KHC, KLC, and several additional proteins (Verhey and Rapoport 2001). Whether these proteins affect the cooperation between KHC motors is an open question.

Finally, we note recent experiments demonstrating that MTs rotate about their axes with a spatial period of 8 μm during kinesin gliding assays (Nitzsche et al. 2008). Whether this also occurs in cells is unknown. Two observations suggest that the beads in our experiments do not rotate about the MT axis. The first is that no lateral oscillation of the beads was detected. The second is that the gliding velocity of MTs with and without a bead was the same in the absence of xanthan (Fig. 4), suggesting that the bead was not experiencing significant friction as it moved with the MT along the casein-coated surface of the coverslip.

## Appendix: Comparison of the viscoelastic properties of xanthan and live cell cytoplasm

In vitro experiments to test motor proteins should be carried out against an external force similar to the one they experience in cells. In our opinion, the load in cells is largely viscoelastic. In this appendix, we provide $G'$ and $G''$ data for 2 mg/ml xanthan solutions, PC12 cells, and NT2 cells. In each case, $G'$ and $G''$ were determined by GSE analysis of the Brownian motion of beads or vesicles of similar size.

Xanthan solutions

Conventional rheological experiments show that dilute xanthan solutions are strongly shear-thinning (Holzwarth 1981; Jeanes et al. 1961; Milas et al. 1985; Rodd et al. 2000) and elastic (Milas et al. 1990; Rochefort and Middleman 1987; Thurston and Pope 1981). Rather than assuming that these data apply to small beads, we measured the complex shear modulus $G*$ from the Brownian

motion of 2-μm beads in the same xanthan solutions used in our motility assays (Figs. 4, 5). The real and the imaginary parts of $G*$, which measure the elastic and viscous responses of the fluid (Tschoegl 1989), are shown in Fig. 11, left panel, for 2-μm beads in a 2 mg/ml xanthan solution. The viscous and elastic components are of similar magnitude. As a control, $G'$ and $G''$ were also determined for 2-μm beads in water. At low shear rate, the viscous factor $G''$ for water was 1/1,000th the value of the $G''$ for the xanthan solution. The elastic part of $G*$ for water was
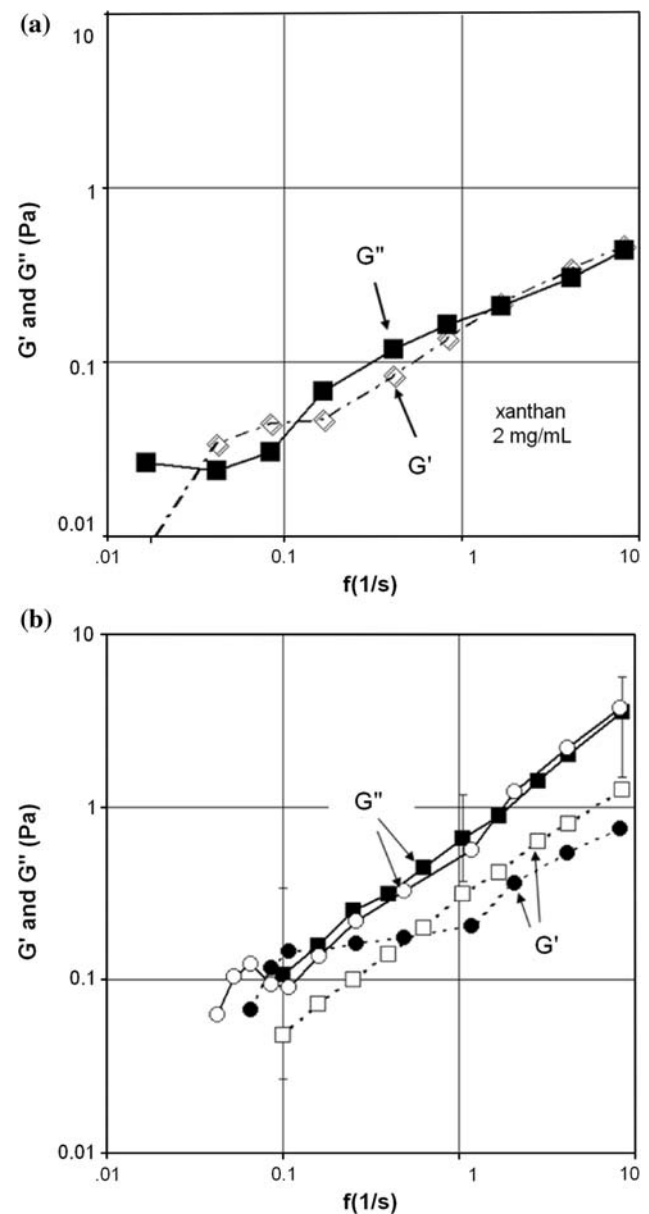


**Fig. 11** Viscoelastic properties of beads in xanthan solutions (*panel* **a**) and vesicles in cytoplasm in live PC12 and NT2 cells (*panel* **b**). The data for PC12 are from the dissertation of Hill (2003). The NT2 data are unpublished experiments of Shtridelman (see Shtridelman et al. 2008)

much smaller than the viscous part for water and could not be reliably measured. This result is not surprising since water is known to be viscous but not elastic.

## Live cells

The values of $G'$ and $G''$ for the cytoplasm of live PC12 and NT2 cells were determined from the Brownian motion of *endogenous* organelles with radius 0.2–0.8 μm (Fig. 11, right panel). For live cells, motor-driven rather than thermally diffusing vesicles had to be excluded, which was easily done by inspecting the path; if the particle went in the same direction for more than 1 s (8 frames), it was excluded. The values of $G'$, the elastic component, were similar to one another for the two cell lines and also close to the values for 2 mg/ml xanthan. The values of $G''$, the viscous component, were about threefold larger for the two live cell lines than for xanthan. Both cell lines and xanthan exhibit shear-thinning (slope < 1), but the xanthan solutions are more shear-thinning than cytoplasm for these two cell lines.

## References

Allen RD, Metuzals J, Tasaki I, Gilbert SP (1982) Fast axonal transport in squid giant axon. Science 218:1127–1128

Ashkin A, Schuetze K, Dziedzic JM, Euteneuer U, Schliwa M (1990) Force generation of organelle transport measured in vivo by an infrared laser trap. Nature 348:346–348

Ausserre D, Hervet H, Rondelez F (1986) Concentration dependence of the interfacial depletion layer thickness for polymer solutions in contact with nonadsorbing walls. Macromolecules 19:85–88

Beeg J, Klumpp S, Dimova R, Garcia RS, Unger E (2008) Transport of beads by several kinesin motors. Biophys J 94:532–541

Bevington PR (1969) Data reduction and error analysis for the physical sciences. McGraw-Hill, New York

Bieling P, Telley IA, Piehler J, Surrey T (2008) Processive kinesins require loose mechanical coupling for efficient collective motility. EMBO Rep 9:1121–1127

Block SM, Goldstein LSB, Schnapp BJ (1990) Bead movement by single kinesin molecules studied with optical tweezers. Nature 348:348–352

Cai D, Verhey KJ, Meyerhofer E (2007) Tracking single kinesin molecules in the cytoplasm of mammalian cells. Biophys J 92:4137–4144

Carter NJ, Cross RA (2005) Mechanics of the kinesin step. Nature 435:308–312

Chisena EN, Wall RA, Macosko JC, Holzwarth GM (2007) Speckled microtubules improve tracking in motor-protein gliding assays. Phys Biol 7:10–15

Coppin CM, Pierce DW, Hsu L, Vale RD (1997) The load dependence of kinesin's mechanical cycle. Proc Nat Acad Sci USA 94:8539–8544

Coy DL, Wagenbach M, Howard J (1999) Kinesin takes one 8-nm step for each ATP that it hydrolyzes. J Biol Chem 274:3667–3671

Crevenna AH, Madathil S, Cohen DN, Wagenbach M, Fahmy K, Howard J (2008) Secondary structure and compliance of a predicted flexible domain in kinesin-1 necessary for cooperation of motors. Biophys 95:5216–5227

Dubois M, Gilles KA, Hamilton JK, Rebers PA, Smith F (1956) Colorimetric method for determination of sugars and related substances. Anal Chem 28:350–356

Gibbons F, Chauwin J-F, Desposito M, Jose JV (2001) A dynamic model of kinesin-microtubule motility assays. Biophys J 80:2515–2526

Hackney DD (1995) Highly processive microtubule-stimulated ATP hydrolysis by dimeric kinesin head domains. Nature 377:448–451

Hill DB (2003) Changes in the number of molecular motors driving vesicle transport in PC12 physics. Wake Forest University, Winston-Salem, pp 120

Hill DB, Plaza MJ, Bonin KD, Holzwarth G (2004) Fast vesicle transport in PC12 neurites: velocities and forces. Eur Biophys J 33:623–632

Holzwarth G (1976) Conformation of the extracellular polysaccharide of xanthomonas campestris. Biochemistry 15:4333–4339

Holzwarth GM (1981) Is xanthan a wormlike chain or a rigid rod? In: Brant DA (ed) Solution properties of polysaccharides, vol. 150. ACS, Houston, pp 15–23

Holzwarth G, Bonin K, Hill DB (2002) Forces required of kinesin during processive transport through cytoplasm. Biophys J 82:1784–1790

Howard J, Hudspeth AJ, Vale RD (1989) Movement of microtubules by single kinesin molecules. Nature 342:154–158

Hunt AJ, Gittes F, Howard J (1994) The force exerted by a single kinesin molecule against a viscous load. Biophys J 67:766–781

Jeanes A, Pittsley JE, Senti FR (1961) Polysaccharide B-1459: a new hydrocolloid polyelectrolyte produced from glucose by bacterial fermentation. J Appl Polym Sci 5:319–326

Kaiser AE, Graham AL, Mondy LA (2004) Non-Newtonian wall effects in concentrated suspensions. J Non-Newton Fluid Mech 116:479–488

Kerssemakers J, Howard J, Hess H, Diez S (2006) The distance that kinesin-1 holds its cargo from the microtubule surface measured by fluorescence interference contrast microscopy. Proc Natl Acad Sci USA 103:13812–13817

Klumpp S, Lipowsky R (2005) Cooperative cargo transport by several molecular motors. Proc Nat Acad Sci USA 102:17284–17289

Klumpp LM, Hoenger A, Gilbert SP (2004) Kinesin's second step. Proc Natl Acad Sci USA 101:3444–3449

Kojima H, Muto E, Higuchi H, Yanagida T (1997) Mechanics of single kinesin molecules measured by optical trapping nanometry. Biophys J 73:2012–2022

Kunwar A, Vershinin M, Xu J, Gross SP (2008) Stepping, strain gating, and an unexpected force-velocity curve for multiple-motor-based transport. Curr Biol 18:1173–1183

Kural C, Kim H, Syed S, Goshima G, Gelfand VI, Selvin PR (2005) Kinesin and dynein move a peroxisome in vivo: a tug-of-war of coordinated movement? Science 308:1469–1472

Leduc C, Campas O, Zeldovich KB, Roux A, Jolimaitre P, Borel-Bonnet L, Goud B, Joanny J-F, Prost J (2004) Cooperative extraction of membrane nanotubes by molecular motors. Proc Nat Acad Sci USA 101:17096–17101

Leduc C, Ruhnow F, Howard J, Diez S (2007) Detection of fractional steps in cargo movement by the collective operation of kinesin-1 motors. Proc Natl Acad Sci USA 104:10847–10852

Levi V, Serpinskaya AS, Gratton E, Gelfand V (2006) Organelle transport along microtubules in *Xenopus melanophores*: evidence for cooperation between multiple motors. Biophys J 90:318–327

Luby-Phelps K (2000) Cytoarchitecture and physical properties of cytoplasm: volume, viscosity, diffusion, intracellular surface area. Int Rev Cytol 192:189–221

Macosko JC, Newbern JM, Rockford J, Chisena EN, Brown CM, Holzwarth GM, Milligan CE (2008) Fewer active motors per

vesicle explains slowed vesicle transport in chick motoneurons after three days in vitro. Brain Res 1211:6–12

Mason TG (2000) Estimating the viscoelastic moduli of complex fluids using the generalized Stokes-Einstein equation. Rheol Acta 39:371–378

Milas M, Rinaudo M, Tinland B (1985) The viscosity dependence on concentration, molecular weight, and shear rate of xanthan solutions. Polym Bull 14:157–164

Milas M, Rinaudo M, Knipper M, Schuppiser JL (1990) Flow and viscoelastic properties of xanthan gum solutions. Macromolecules 23:2506–2511

Nan X, Sims PA, Xie XS (2008) Organelle tracking in a living cell with microsecond time resolution and nanometer spatial precision. Chemphyschem 2008:707–712

Nishiyama M, Muto E, Inoue Y, Yanagida T, Higuchi H (2001) Substeps within the 8-nm step of the ATPase cycle of single kinesin molecules. Nat Cell Biol 3:425–428

Nitzsche B, Ruhnow F, Diez S (2008) Quantum-dot-assisted characterization of microtubule rotations during cargo transport. Nat Nanotechnol 3:552–556

Rochefort WE, Middleman S (1987) Rheology of xanthan gum: salt, temperature, and strain effects in oscillatory and steady shear experiments. J Rheol 31:337–369

Rodd AB, Dunstan DE, Boger DV (2000) Characterisation of xanthan gum solutions using dynamic light scattering and rheology. Carbohydr Polym 42:159–174

Rogers AR, Driver JW, Constantinou PE, Jamison DK, Diehl MR (2009) Negative interference dominates collective transport of kinesin motors in the absence of load. Phys Chem Chem Phys 11:4882–4889

Schliwa M (2003) Molecular motors. Wiley-VCH, Weinheim

Shtridelman Y, Cahyuti T, Townsend B, DeWitt D, Macosko JC (2008) Force-velocity curves of motor proteins cooperating in vivo. Cell Biochem Biophys 52:19–29

Shtridelman Y, Holzwarth GM, Bauer CT, Gassman NR, DeWitt DA, Macosko JC (2009) In vivo multimotor force-velocity curves by tracking and sizing sub-diffraction limited vesicles. Cell Mol Bioeng 2:190–199

Shubeita GT, Tran SL, Xu J, Vershinin M, Cermelli S, Cotton SL, Welte MA, Gross SP (2008) Consequences of motor copy number on the intracellular transport of kinesin-1-driven lipid droplets. Cell 135:1098–1107

Svoboda K, Schmidt CF, Schnapp BJ, Block SM (1993) Direct observation of kinesin stepping by optical trapping interferometry. Nature 365:721–727

Thomas RH, Walters K (1965) The unsteady motion of a sphere in an elastico-viscous liquid. Rheol Acta 5:23–27

Thurston GB, Pope GA (1981) Shear rate dependence of the viscoelasticity of polymers solutions. 2. Xanthan gum. J Non-Newton Fluid Mech 9:69–78

Tschoegl NW (1989) The phenomenological theory of linear viscoelastic behavior. Springer, Berlin

Verhey KJ, Rapoport TA (2001) Kinesin carries the signal. Trends Biochem Sci 26:545–549

Visscher K, Schnitzer MJ, Block SM (1999) Single kinesin molecules studied with a molecular force clamp. Nature 400:184–189

Walker RA, O'Brien ET, Pryer NK, Soboeiro MF, Voter WA, Erickson HP, Salmon ED (1988) Dynamic instability of individual microtubules analyzed by video light microscopy: rate constants and transition frequencies. J Cell Biol 107:1437–1448

Waterman-Storer CM, Salmon ED (1998) How microtubules get fluorescent speckles. Biophys J 75:2059–2069

Welte MA, Gross S, Postner M, Block S, Wieschaus E (1998) Developmental regulation of vesicle transport in *Drosophila* embryos: forces and kinetics. Cell 92:547–557

Zhou MH, Mascher IB, Scholey JM (2001) Direct visualization of the movement of the monomeric axonal transport motor UNC-104 along neuronal processes in living *Caenorhabditis elegans*. J Neurosci 21:3749–3755